# Amyloid, Tau, and APOE in Alzheimer's Disease: Impact on White Matter Tracts

Bramsh Qamar Chandio[1†], Julio E. Villalon-Reina[1], Talia M. Nir[1], Sophia I. Thomopoulos[1], Yixue Feng[1], Sebastian Benavidez[1], Neda Jahanshad[1], Jaroslaw Harezlak[2], Eleftherios Garyfallidis[2], and Paul M. Thompson[1]

[1]*Imaging Genetics Center, Mark and Mary Stevens Neuroimaging and Informatics Institute, Keck School of Medicine, University of Southern California, Marina del Rey, CA, USA*

[2]*Indiana University Bloomington, IN, USA.* [†]*E-mail: chandio@usc.edu*

Alzheimer's disease (AD) is characterized by cognitive decline and memory loss due to the abnormal accumulation of amyloid-beta (A$\beta$) plaques and tau tangles in the brain; its onset and progression also depend on genetic factors such as the apolipoprotein E (APOE) genotype. Understanding how these factors affect the brain's neural pathways is important for early diagnostics and interventions. Tractometry is an advanced technique for 3D quantitative assessment of white matter tracts, localizing microstructural abnormalities in diseased populations *in vivo*. In this work, we applied BUAN (Bundle Analytics) tractometry to 3D diffusion MRI data from 730 participants in ADNI3 (phase 3 of the Alzheimer's Disease Neuroimaging Initiative; age range: 55-95 years, 349M/381F, 214 with mild cognitive impairment, 69 with AD, and 447 cognitively healthy controls). Using along-tract statistical analysis, we assessed the localized impact of amyloid, tau, and APOE genetic variants on the brain's neural pathways. BUAN quantifies microstructural properties of white matter tracts, supporting along-tract statistical analyses that identify factors associated with brain microstructure. We visualize the 3D profile of white matter tract associations with tau and amyloid burden in Alzheimer's disease; strong associations near the cortex may support models of disease propagation along neural pathways. Relative to the neutral genotype, APOE $\epsilon3/\epsilon3$, carriers of the AD-risk conferring APOE $\epsilon4$ genotype show microstructural abnormalities, while carriers of the protective $\epsilon2$ genotype also show subtle differences. Of all the microstructural metrics, mean diffusivity (MD) generally shows the strongest associations with AD pathology, followed by axial diffusivity (AxD) and radial diffusivity (RD), while fractional anisotropy (FA) is typically the least sensitive metric. Along-tract microstructural metrics are sensitive to tau and amyloid accumulation, showing the potential of diffusion MRI to track AD pathology and map its impact on neural pathways.

*Keywords*: diffusion MRI, tractometry, Alzheimer's disease, amyloid, tau

## 1. Introduction

Alzheimer's disease (AD) is a neurodegenerative disorder characterized by progressive cognitive decline and memory loss. Central to its pathology are the abnormal accumulation of amyloid-beta ($A\beta$) plaques and tau tangles in the brain.[1–3] The onset and progression of these pathological processes are influenced by genetic factors such as the apolipoprotein E (APOE) gene.[4] AD pathology not only affects gray matter but also profoundly impacts white matter tracts, which serve as the brain's communication mechanism; these tracts connect different

brain regions and facilitate efficient signal transmission. Understanding how amyloid, tau, and APOE influence white matter integrity is crucial for developing early diagnostic tools and monitoring effects of targeted interventions on the brain.

Amyloid-beta peptides aggregate to form plaques, primarily affecting gray matter[5] but also extending to white matter tracts by disturbing cellular function.[6,7] $A\beta$ deposition leads to myelin degradation, which disrupts the insulating layer around nerve fibers, and axonal injury, which impairs neurons' ability to communicate effectively. The presence of $A\beta$ can trigger a chronic inflammatory response, worsening white matter damage through microglial activation and the release of pro-inflammatory cytokines.

Tau is a microtubule-associated protein that stabilizes microtubules in neurons. In AD, tau becomes hyperphosphorylated and forms neurofibrillary tangles,[8] affecting microtubule stability, disrupting axonal transport and, impairing neuronal function. The propagation of tau pathology correlates with synaptic loss and neuronal degeneration, affecting both gray and white matter regions and leading to widespread brain dysfunction.[9,10]

The apolipoprotein E (APOE) gene has three common variants: $\epsilon 2$, $\epsilon 3$, and $\epsilon 4$. APOE $\epsilon 2$ is the least common, and carriers have a lower risk of developing AD. It may have a protective effect on white matter structure,[11,12] leading to less degeneration compared to those with APOE $\epsilon 3$ or $\epsilon 4$, possibly due to enhanced lipid metabolism and repair mechanisms. APOE $\epsilon 3$ is the most common variant and is considered neutral, while the APOE $\epsilon 4$ variant is the greatest known common genetic risk factor for late-onset AD, roughly tripling lifetime risk of AD per allele carried.[13] APOE $\epsilon 4$ is less effective in clearing $A\beta$ from the brain, leading to greater $A\beta$ plaque accumulation and subsequent white matter damage.[14] APOE is involved in lipid transport and metabolism, essential for myelin maintenance. The $\epsilon 4$ variant affects these processes, leading to compromised myelin maintenance. APOE $\epsilon 4$ carriers also exhibit increased inflammation and vascular dysfunction, contributing to white matter lesions and impaired cerebral blood flow. Even so, relatively little is known about the 3D profile of APOE effects on white matter microstructure.

Investigating the impact of amyloid, tau, and APOE on white matter is vital for advancing AD research and treatment. White matter metrics may deteriorate before gray matter atrophy and clinical symptoms appear, making them a potential biomarker for early detection or monitoring interventions. Diffusion MRI, being less invasive than PET, could offer a better alternative for tracking disease progression if metrics sensitive to these pathologies are identified. Identifying white matter tracts affected may also help to evaluate targeted therapies to protect or restore these pathways. Furthermore, understanding how different APOE genotypes affect white matter may lead to personalized therapeutic strategies, improving outcomes for individuals with specific genetic profiles.

Diffusion MRI[15–17] measures water diffusion in the brain, revealing the microstructural properties of the underlying tissue. Tractography, derived from diffusion MRI data,[18–20] maps and visualizes white matter pathways by tracking the directional profiles of water diffusion, providing a detailed picture of brain connectivity. Tractometry enhances this by quantifying specific microstructural properties, such as fractional anisotropy (FA) or mean diffusivity (MD), along the length of individual tracts. This technique maps microstructural alterations

in the brain's white matter tracts.[21–25] It analyzes the coherence of neural connections, allowing for precise assessment of characteristic changes in neurological conditions such as Alzheimer's disease or Parkinson's disease.[26]

White matter (WM) microstructure changes with age, and there is a regional variation in the age-dependent trajectories of maturation and decline for the major white matter metrics across the lifespan.[27,28] Several studies of regional microstructure in Alzheimer's disease have used tract-based spatial statistics (TBSS),[29] to link microstructural metrics in specific brain regions to amyloid positivity and clinical dementia severity.[30–32] However, the resolution of TBSS maps is limited by the regions defined in the atlases used.[29] To address this, tractometry methods such as BUAN (Bundle Analytics)[33] map microstructural parameters along the length of white matter tracts, mapping disease effects on neural pathways in 3D and at a finer anatomical scale.[23,25,26,34,35] Recently, Ba Gari *et al.*[34] used a tractography-based medial tract analysis (MeTa) to enhance the sensitivity for detecting associations of AD, amyloid and tau with DTI microstructural metrics, compared to TBSS.

In this study, we applied our advanced tractometry method, BUAN (Bundle Analytics), to evaluate the impact of amyloid, tau, APOE $\epsilon 4$, and APOE $\epsilon 2$ on the microstructure of the brain's white matter tracts. BUAN maps the microstructural properties of white matter tracts, and fits along-tract statistical models to detect effects on microstructure that are associated with amyloid plaques, tau tangles, and different APOE genotypes. This is crucial for understanding the effects of AD pathology on brain connectivity. Overall, we found that a range of microstructural metrics were sensitive to tau and amyloid, the two key biomarkers for detecting Alzheimer's disease, supporting the role of diffusion MRI as a non-invasive measure of AD pathology. Relative to APOE $\epsilon 3/\epsilon 3$ carriers, microstructural alterations were also identified in APOE $\epsilon 4$ carriers, and to a less extent in $\epsilon 2$ carriers.

Overall, mean diffusivity (MD) was most strongly associated with AD pathology, followed by axial diffusivity (AxD) and radial diffusivity (RD). Fractional anisotropy (FA) was the least sensitive metric. The tendency to detect stronger associations in tract regions closer to the cortex may support propagative or "epidemic spreading" models of AD pathology,[36] which argue that AD pathology spreads dynamically along neural pathways or in functionally synchronous networks; future longitudinal studies are needed to verify this.

## 2. Methods

### 2.1. *Data*

Data from 730 ADNI3 participants (phase 3 of the Alzheimer's Disease Neuroimaging Initiaitve; age range: 55-95 years, 349M/381F, 214 with mild cognitive impairment (MCI), 69 with AD, and 447 cognitively healthy controls (CN)) scanned with 7 acquisition protocols (GE36, GE54, P33, P36, S127, S31, S55) were included. Tables 1 and 2 in Fig. 2 detail demographic and acquisition protocol information. A$\beta$-status, i.e., positive (A$\beta$+) or negative (A$\beta$–), was determined by either mean 18F-florbetapir (A$\beta$+ defined as >1.11)[37,38] or florbetaben (A$\beta$+ defined as >1.20)[39,40] PET cortical SUVR uptake, normalized by using a whole cerebellum reference region. Tau positivity was defined as a tau SUVR > 1.23.

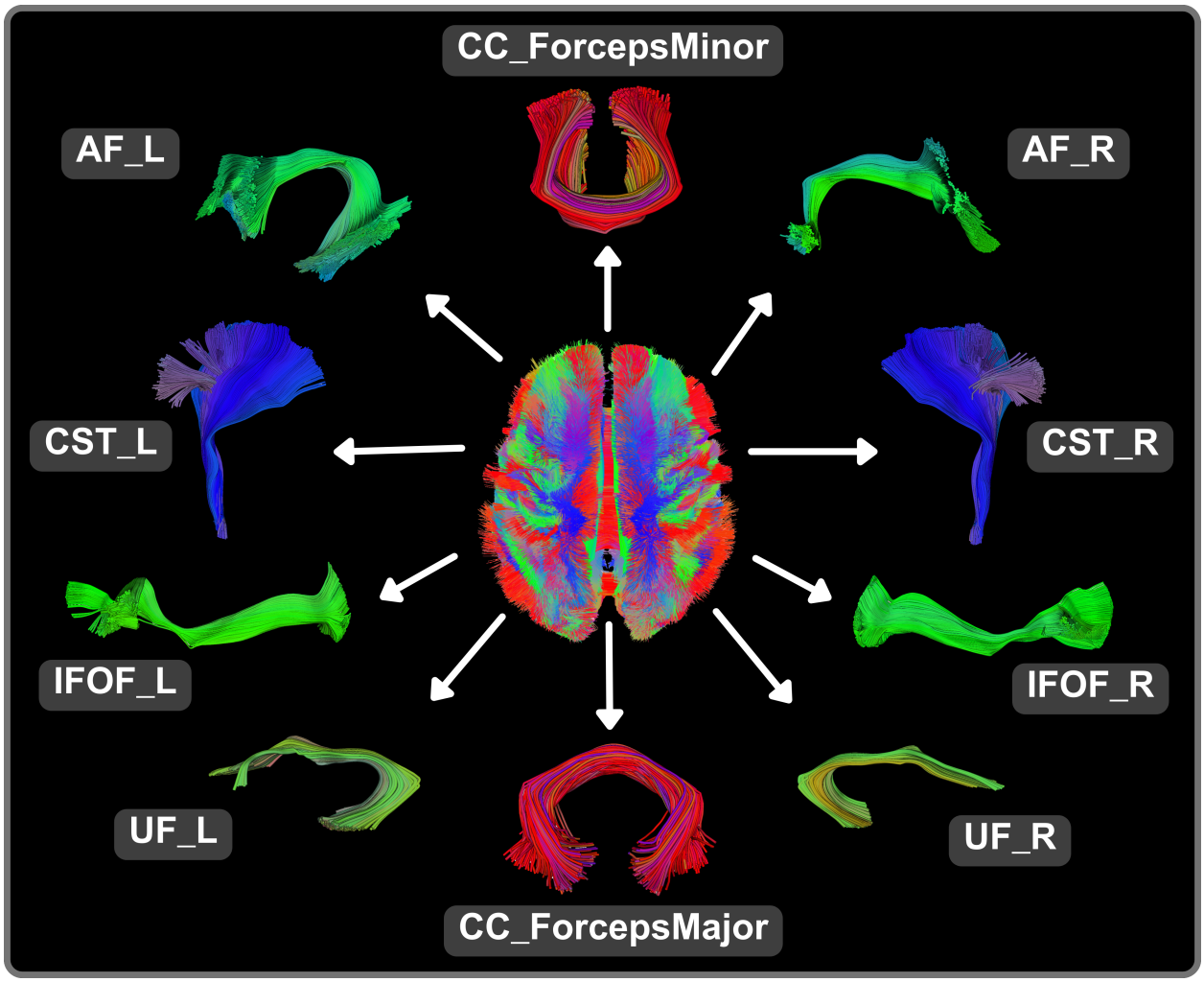


Fig. 1. The brain contains millions of axonal connections; the trajectories of the major neural pathways can be digitally reconstructed into a whole brain tractogram using diffusion MRI and tractography techniques. Specific white matter tracts are extracted for visualization and detailed analysis, offering a more localized and focused examination of pathways within the brain.

### 2.2. *Diffusion MRI Processing*

Raw diffusion MRI (dMRI) were preprocessed using the ADNI3 dMRI protocol.[41,42] Preprocessing of raw diffusion MRI (dMRI) data involved several steps: denoising raw dMRI data using DIPY's principal component analysis (PCA) for GE data, and Marchenko-Pastur PCA for Siemens and Philips data denoising.[43,44] Gibbs artifacts were corrected using MRtrix's *degibbs* tool,[45,46] and extracerebral tissue was removed (skull stripping) with FSL's BET.[47,48] Eddy currents and motion were corrected using FSL's eddy_cuda tool with additional corrections for slice-to-volume and outlier detection.[48,49] Bias field inhomogeneities were corrected using MRtrix's *dwibiascorrection* ANTS function. Preprocessed T1w images from the ADNI database were further processed and aligned to the dMRI data.[46,50] ADNI3 dMRI data lacked

**Table 1**. Participant demographics. 'Site N' denotes the number of sites across North America using the dMRI acquisition protocol specified (protocols are further detailed in **Table 2**). * NB: some sites collected data with more than one protocol, so the total number of sites is less than the sum of the final column.

| Protocol | Total N | Diagnosis | | | M | F | Age | CDR-sob | Amyloid | | Tau | | Site N* |
|---|---|---|---|---|---|---|---|---|---|---|---|---|---|
| | | CN | MCI | Dementia | | | (Mean±SD) | (Mean±SD) | Aβ+ | Aβ- | Tau+ | Tau- | |
| **S55** | 270 | 175 | 71 | 24 | 120 | 150 | 74.4±7.9 | 0.93±2.0 | 103 | 117 | 67 | 141 | 18 |
| **S31** | 96 | 59 | 27 | 10 | 39 | 57 | 72.0±8.5 | 0.96±1.8 | 26 | 49 | 21 | 56 | 10 |
| **S127** | 112 | 68 | 36 | 8 | 53 | 59 | 73.7±7.6 | 0.78±1.5 | 35 | 58 | 21 | 67 | 14 |
| **P36** | 46 | 20 | 23 | 3 | 24 | 22 | 73.1±6.9 | 0.84±1.1 | 12 | 27 | 15 | 22 | 5 |
| **P33** | 56 | 37 | 14 | 5 | 34 | 22 | 75.7±7.7 | 1.03±2.1 | 19 | 21 | 11 | 26 | 6 |
| **GE36** | 42 | 21 | 17 | 4 | 24 | 18 | 72.2±7.1 | 1.29±2.7 | 13 | 22 | 9 | 26 | 4 |
| **GE54** | 108 | 67 | 26 | 15 | 55 | 53 | 76.1±8.1 | 1.16±2.0 | 37 | 57 | 24 | 63 | 10 |
| **Total** | **730** | **447** | **214** | **69** | **349** | **381** | **74.1±7.9** | **0.97±1.9** | **245** | **351** | **168** | **401** | **58** |

**Table 2.** ADNI3 dMRI acquisition protocols.

| Protocol | Scanner | | Volumes | | | Matrix | Acquisition Time (min:sec) |
|---|---|---|---|---|---|---|---|
| | Vendor | Model | $b_0$ | DWI | Total | | |
| **GE36** | GE | Basic Widebore 25x | 4 b=0 s/mm$^2$ | 32 b=1000 s/mm$^2$ | 36 | 256x256 | 9:52 |
| **GE54** | GE | Basic 25x | 6 b=0 s/mm$^2$ | 48 b=1000 s/mm$^2$ | 54 | | 7:09 |
| **P33** | Philips | Basic Widebore | 1 b=0 s/mm$^2$ | 32 b=1000 s/mm$^2$ | 33 | 128x128 | 7:32 |
| **P36** | Philips | Basic Widebore R3 | 1 b=0 s/mm$^2$<br>3 b=2 s/mm$^2$ | 32 b=1000 s/mm$^2$ | 36 | | 6:54 |
| **S31** | Siemens | Basic VB17 | 1 b=0 s/mm$^2$ | 30 b=1000 s/mm$^2$ | 31 | 116x116 | 7:02 |
| **S55** | Siemens | Basic Skyra E11 & Prisma D13 | 7 b=0 s/mm$^2$ | 48 b=1000 s/mm$^2$ | 55 | | 9:18 |
| **S127** | Siemens | Advanced Prisma VE11C | 13 b=0 s/mm$^2$ | 6 b=500 s/mm$^2$<br>48 b=1000 s/mm$^2$<br>60 b=2000 s/mm$^2$ | 127 | | 7:25* |

**Abbreviations**

| | |
|---|---|
| Left/Right (L/R) | Anterior Commissure (AC) |
| Corticospinal Tract (CST) | Corpus Callosum Mid (CCMid) |
| Fornix (F) | CC Forceps_Minor |
| Optic Radiation (OR) | CC Forceps_Major |
| Frontopontine Tract (FPT) | Posterior Commissure (PC) |
| Occipitopontine Tract (OPT) | Cerebellum (CB) |
| Cingulum (C) | Vermis (V) |
| Arcuate Fasciculus (AF) | Medial Lemniscus (ML) |
| Extreme Capsule (EMC) | Medial Longitudinal Fasciculus (MLF) |
| Inferior Fronto Occipital Fasciculus (IFOF) | Spinothalamic Tract (STT) |
| Inferior Longitudinal Fasciculus (ILF) | Fractional Anisotropy (FA) |
| Middle Longitudinal Fasciculus (MdLF) | Mean Diffusivity (MD) |
| Superior Longitudinal Fasciculus (SLF) | Axial Diffusivity (AD) |
| Uncinate Fasciculus (UF) | Radial Diffusivity (RD) |

Fig. 2. Tables 1 and 2 detail demographic and scanner protocol information for the ADNI3 data used in our experiments (data from Thomopoulos et al, 2021). The abbreviation table on the right lists the 38 white matter tracts and four microstructural measures analyzed in this work.

reversed phase-encode blips, so echo-planar imaging (EPI) distortion corrections were made using nonlinear registrations to T1-weighted anatomical images. The processed dMRI data were converted back to native space through a series of inversions of the registration matrices, with final outputs visually inspected and manually adjusted as necessary. The diffusion tensor imaging (DTI) model was used to extract 4 microstructural measures from processed dMRI: fractional anisotropy (FA), mean, axial and radial diffusivity (MD, AxD, RD).

### 2.3. *BUAN Tractometry*

We applied a robust and unbiased model-based spherical deconvolution[51] reconstruction method and a probabilistic particle filtering tracking algorithm that uses tissue partial volume estimation (PVE) to reconstruct [52] whole-brain tractograms. For tracking, the seed mask was created from the white matter (WM) PVE (WM PVE $> 0.5$), seed density per voxel was set to 2, and step size was set to 0.5. We extracted 38 white matter (WM) tracts from tractograms using auto-calibrated RecoBundles [23,53] (see Fig. 2 for full names) using model bundles from the HCP-842 tractography atlas.[54]

After extracting WM bundles, we nonlinearly registered each subject's bundles to model bundles in MNI-space using a streamline-based nonlinear registration method, BundleWarp.[55] Optimal registration of tracts to atlas bundles is crucial for finding accurate segment correspondences among subjects and populations. This enhances the sensitivity of group statistical analyses by eliminating errors due to misalignment across subjects.

BUAN creates the bundle profiles for each bundle using 4 DTI-based microstructural metrics: FA, MD, RD, and AxD calculated in the diffusion native space (see Figure 2 for full bundle names). Bundle profiles are created by dividing the bundles into 100 horizontal

segments using the model bundle centroids along the length of the tracts in common space. We cluster our model bundles using the QuickBundles[56] method to obtain a cluster centroid consisting of 100 points per centroid. We calculate Euclidean distances between every point on every streamline of the bundle and 100 points in the model bundle centroid. A segment number is assigned to each point in a bundle based on the shortest distance to the nearest model centroid point. The streamlines are not resampled to have a specific number of points, and we do not change the distribution of points. Since the assignment of segment numbers is performed in the common space, we establish the segment correspondence among subjects from different groups and populations. Microstructural measures such as FA are then projected onto the points of the bundles in native space. Note that the nonlinearly moved bundles are only used to assign segment numbers to streamlines (and points on the streamlines) in the bundles. Actual statistical analysis always takes place in the native space of the diffusion data. The statistical analysis step uses bundles of the original shape and microstructural measures in the native space using segment labels given during the assignment step for segment-specific group analysis.

Bundle profiles are harmonized using the ComBat method[57,58] to correct for scanner/site effects as described in the harmonized BUAN tractometry pipeline.[59] After data harmonization, we assume each bundle type has its own data distribution, which is considered independent of the rest of the bundles in the brain. For each tract and metric, we pool bundle profiles for a given tract across all subjects from CN, MCI, and AD groups. Pooled bundle profiles consist of 100 segments, and each segment is modeled as a feature. Linear Mixed Models are applied to WM bundles; age and sex are modeled as fixed effects and scanner and subject as a random effect term, the response variable being each DTI metric. Though we harmonized the profiles with ComBat, we further account for scanner and/or site effects by adding it as a random term in the linear mixed models (LMMs)[60] to eliminate any remaining artifacts contributed by scanner/site. We used FURY[61] software to visualize tractometry results in this paper.

### 2.4. *Statistics*

We used LMMs to test the effects of amyloid positivity, tau positivity, and different APOE variants on 38 white matter tracts. In each experiment, age and sex were modeled as fixed effects, and the scanner and subject were modeled as random terms.

#### 2.4.1. *Multiple test corrections*

Multiple testing correction is a statistical adjustment process that can controls the rate or likelihood of false positives when performing numerous simultaneous tests.[62] In neuroimaging studies, where thousands of brain regions or voxels are analyzed for significant differences or correlations, this adjustment is crucial. It ensures the integrity and reliability of the results by controlling the overall rate of false positives. Common correction methods include the Bonferroni correction,[63] which is stringent and adjusts the significance threshold by dividing it by the number of tests, and the False Discovery Rate (FDR)[64] method, which limits the proportion of false positives among significant findings. These corrections ensure that detected effects are truly significant and not due to random variation.

As white matter tracts generated by tractography are not as extensively studied as voxel or ROI-based methods, selecting the appropriate multiple testing correction is challenging. We divided each bundle into 100 segments; for tract-specific FDR correction, we use 100 $p$-values per bundle to correct for multiple tests using the FDR method. We refer to this bundle-specific FDR corrected threshold as the local threshold, as it only depends on statistics within that bundle. Additionally, we performed multiple test corrections across all bundles in the brain by pooling 100 $p$values from each of the 38 tracts, yielding a total of 3,800 $p$values to determine the global FDR-corrected threshold. We consider tract effects to be significant if they pass both local and global FDR thresholds.

## 3. Results

We ran the following five experiments to detect associations of various variables on 38 white matter tracts of the brain. We tested microstructural associations (1) with amyloid positivity; (2) with tau positivity; (3) comparing non $\epsilon 4$ carriers $\epsilon 2\epsilon 3/\epsilon 3\epsilon 3/\epsilon 2\epsilon 2$ with subjects carrying at least one $\epsilon 4$ gene; $\epsilon 2\epsilon 4/\epsilon 3\epsilon 4/\epsilon 4\epsilon 4$, (4) comparing $\epsilon 3\epsilon 3$ with $\epsilon 3\epsilon 4/\epsilon 4\epsilon 4$, and (5) comparing $\epsilon 3\epsilon 3$ with $\epsilon 3\epsilon 2/\epsilon 2\epsilon 2$.

As an overview of the results, quantitative quantile-quantile (QQ) plots (Fig. 3) summarize the overall association signal detected across all 38 white matter bundles between each of the biomarkers (amyloid, tau, and APOE) and each of the DTI metrics (FA, MD, RD, and AxD). These plots visually represent the strength of associations between these biomarkers and DTI metrics, helping to identify which combinations show the most significant relationships.

In the visualization layout, the first row of QQ plots highlights which DTI metric exhibits the strongest association with each biomarker. Here, the $p$-values of the 38 tracts were pooled for each DTI metric and presented in these plots, allowing for a comprehensive assessment of each metric's sensitivity to changes in biomarker levels.

The second focuses on the relationship from the opposite perspective: for each DTI metric, which show which biomarker shows significant associations (the scale of the $y$-axis varies across the QQ plots, to adapt to the observed range of $p$-values).

### 3.1. *Amyloid*

We ran BUAN to assess the effect of amyloid positivity on 38 white matter tracts based on data from 329 amyloid-negative (CN: 235, MCI: 86, Dementia: 8) (156M, 173F) and 277 amyloid-positive (CN: 139, MCI : 87, Dementia: 51) (131M, 146F) participants from the ADNI3 dataset.

We found that the following tracts and measures showed significant differences between amyloid negative and amyloid positive: cingulum left (AxD, MD), corpus callosum forceps major and middle sector (MD, RD), extreme capsule left (MD, RD) and right (AxD, MD, RD), frontopontine tract left (AxD, MD) and right (AxD), inferior longitudinal fasciculus right (AxD, MD, RD), middle longitudinal fasciculus left (AxD, MD) and right (AxD, MD, RD), occipito-pontine tract left (MD), optic radiation right (MD), posterior commissure (AxD), and spinothalamic tract left (RD).

In significant tracts, diffusivity metrics increase while fractional anisotropy decreases, in

those with higher levels of amyloid pathology (this is in the same direction as the known effects of dementia on these metrics).

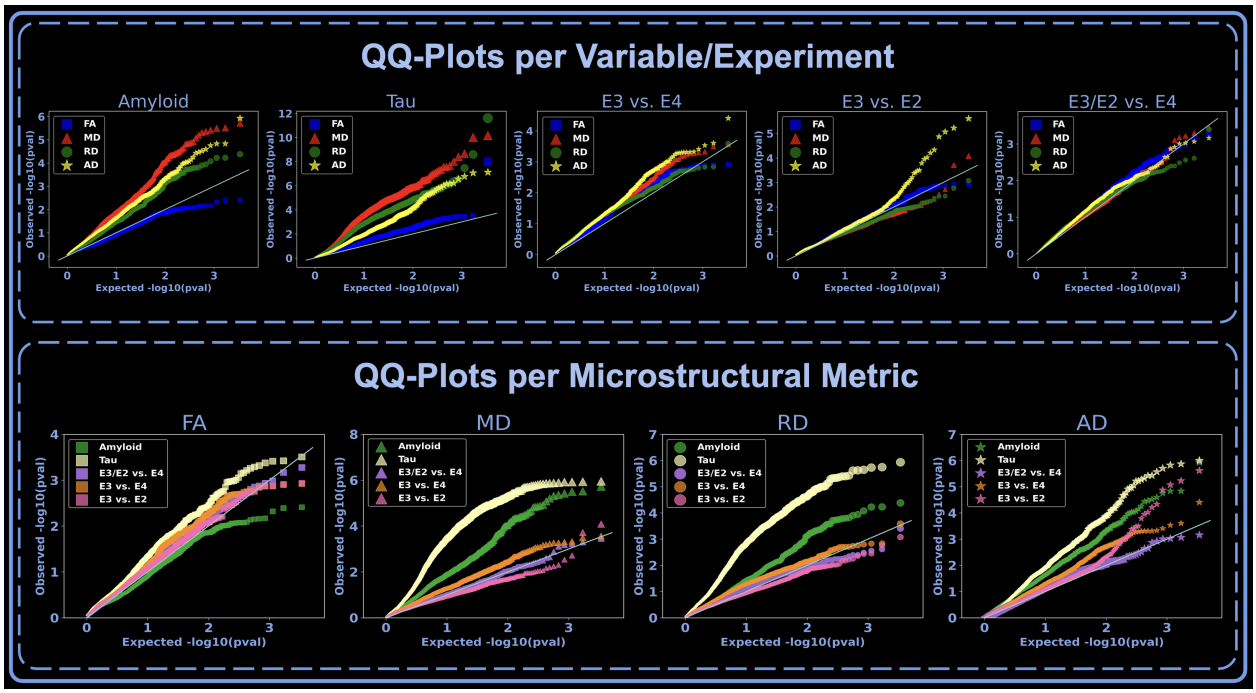


Fig. 3. QQ plots summarize the signal detected by each biomarker (amyloid, tau, and ApoE) and DTI metric (FA, MD, RD, and AxD) across all 38 bundles, indicating which biomarkers and metrics show the strongest associations. In the first row, the plots show which metric shows the strongest association for each biomarker. $P$-values of the 38 tracts were pooled together for each DTI metric and visualized in QQ plots. In the second row, we analyze for each metric which biomarker shows significant associations. Note the $y$-axis range varies across the plots depending on the observed range of $p$-values.

### 3.2. *Tau*

We ran BUAN to assess the effect of tau positivity on 38 white matter tracts based on data from 401 tau-negative (CN: 293, MCI: 95, and Dementia: 13) (192M, 209F) and 168 amyloid-positive (CN: 60, MCI: 68, and Dementia: 40) (75M, 93F) participants in the ADNI3 dataset. The following tracts and measures showed significant associations between tau positivity and microstructure:

Arcuate fasciculus left (MD, RD), cingulum left and right (MD, RD), corpus callosum - forceps major (MD, RD), forceps minor (FA, MD, RD) and mid (AD, MD, RD), corticospinal Tract left and right (MD, RD), extreme capsule left and right (AxD, MD, RD), frontopontine tract left (MD, RD) and right (FA, AxD, MD, RD), inferior fronto-occipital fasciculus right (RD), inferior longitudinal fasciculus left (MD, RD) and right (AxD, MD, RD), middle longitudinal fasciculus left (AxD, MD, RD) and right (AxD, FA, MD, RD), occipito-pontine tract left (MD, RD) and right (AxD, MD, RD), optic radiation left (RD) and right (AxD, MD, RD), and uncinate fasciculus right (MD, RD).

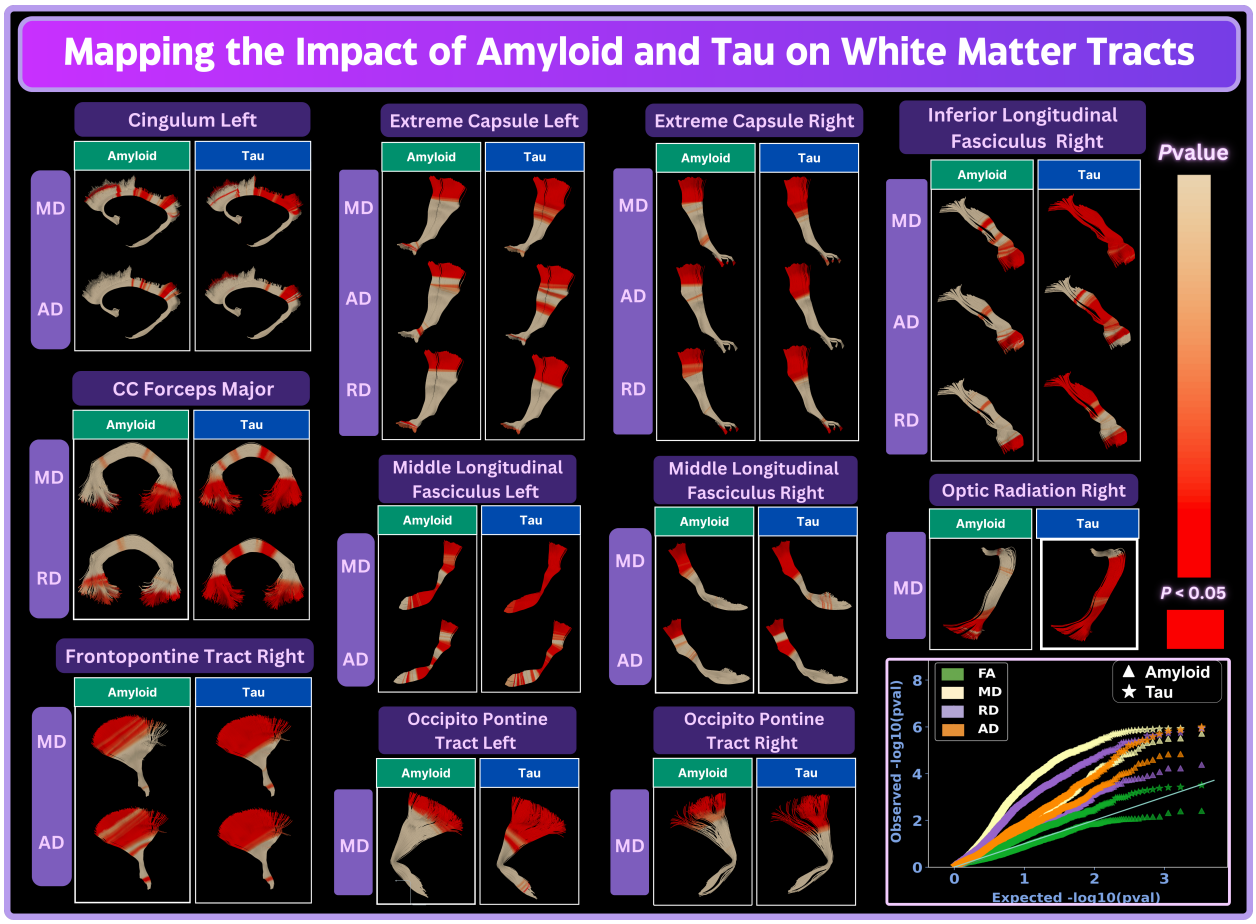


Fig. 4. We compare the effects of amyloid and tau on white matter microstructure along the major white matter tracts. Only tracts showing significant effects, passing both local and global FDR for amyloid and tau, are visualized. *Red* highlights significant associations between the measures of Alzheimer's disease pathology and the microstructural metrics computed with DTI. We consistently observe the strongest associations with tau in various white matter tracts, as seen in the QQ-plot at the right end of the figure. Tau outperforms amyloid in terms of strength of association, for each microstructural metric.

In significant tracts, most diffusivity metrics increase while fractional anisotropy decreases, in line with the expected direction of microstructural abnormalities previously reported in dementia. However, in some tracts, changes in AxD vary along the length of the tracts.

We compare the impact on white matter tracts as influenced by amyloid and tau in Fig. 4. Only those tracts that demonstrate significant effects, meeting both local and global false discovery rate (FDR) criteria for amyloid and tau, are included. Significant associations with each biomarker in conjunction with DTI metrics are highlighted in red. We consistently observe stronger associations with tau across various white matter tracts, as illustrated in the QQ-plot at the right end of the figure. For all metrics assessed, tau shows stronger associations compared to amyloid.

MD metrics exhibit the strongest association signal for both amyloid and tau. We illustrate

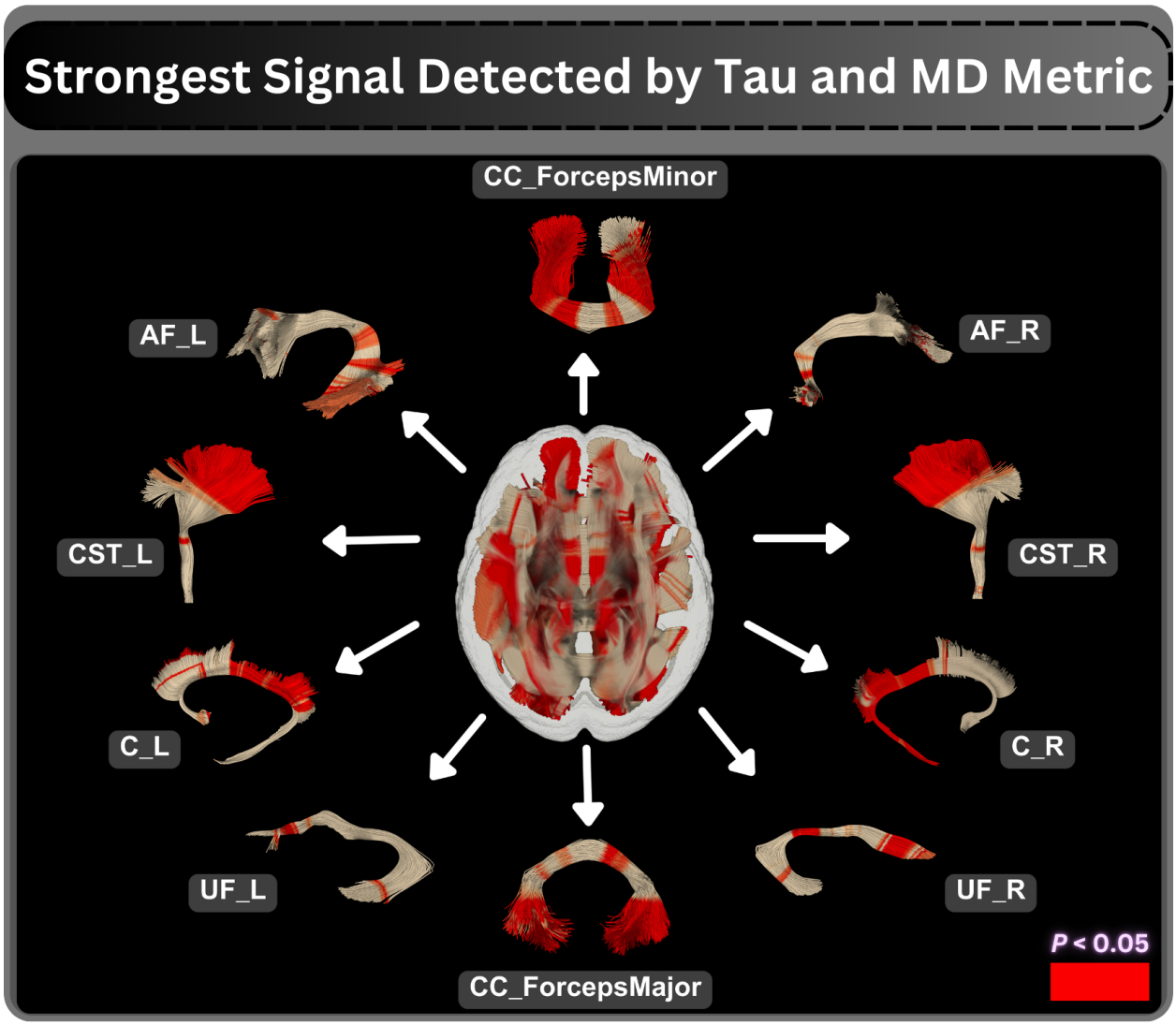


Fig. 5. Visualization of localized effects of Tau on MD metrics detected by BUAN. Each tract is colored based on $p$-values, with red indicating p<0.05. The combination of Tau and MD detects the strongest association signal among amyloid, tau, ApoE, and the four DTI metrics.

the localized effects of tau on MD metrics in Fig. 5. Each tract is color-coded based on $p$-values, with tracts showing $p$-values less than 0.05 highlighted in red.

### 3.3. *APOE $\epsilon 4$ genotype*

We ran BUAN to assess the impact of APOE $\epsilon 4$ - the major common risk gene for late-onset Alzheimer's disease - on 38 major white matter tracts, based on data from 358 non $\epsilon 4$ carriers $\epsilon 2\epsilon 3/\epsilon 3\epsilon 3/\epsilon 2\epsilon 2$ (CN: 224, MCI: 99, Dementia: 35) (168M, 190F) and 203 participants with at least one $\epsilon 4$ gene; $\epsilon 2\epsilon 4/\epsilon 3\epsilon 4/$ $\epsilon 4\epsilon 4$ carriers (CN: 136, MCI: 54, and Dementia: 13) (90M, 108F) participants from the ADNI3 dataset.

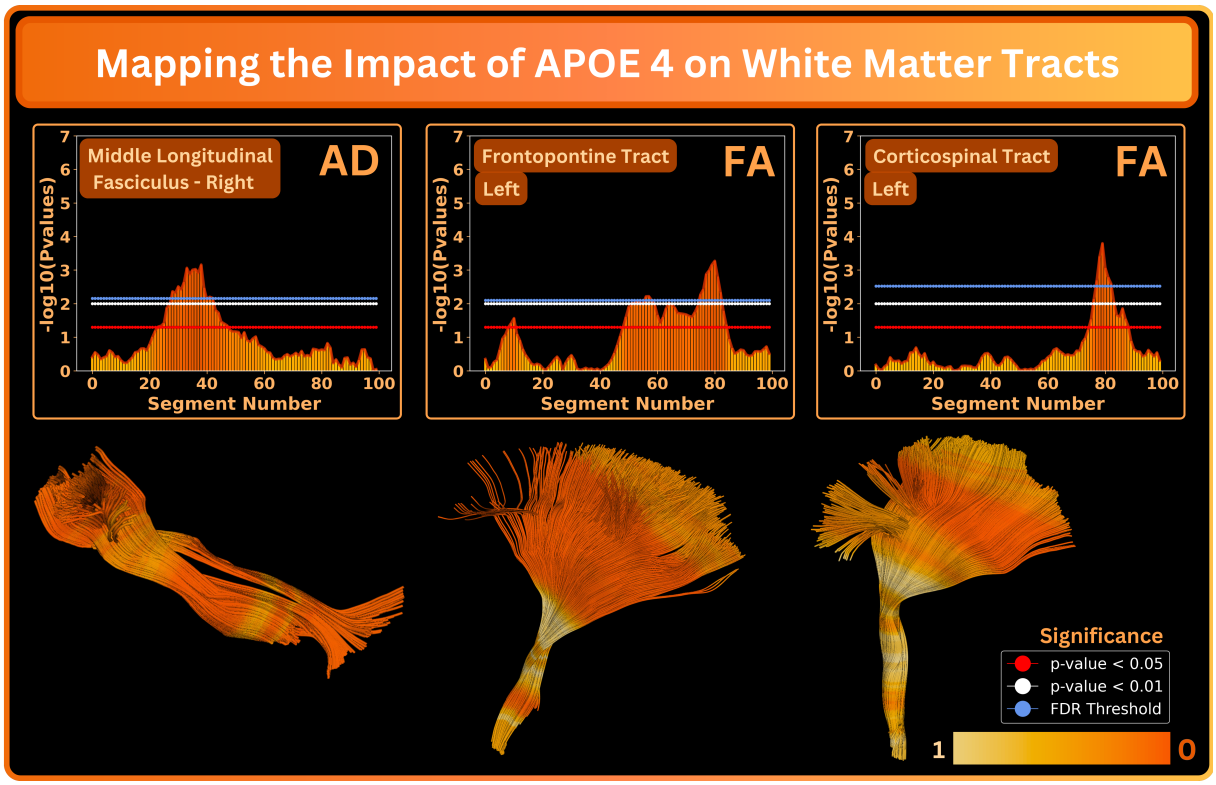


Fig. 6. BUAN results for white matter tracts alteration in the subgroup of participants carrying at least one $\epsilon 4$ gene. The first and third rows show $p$value plots for each tract, where the $x$-axis represents the segment number along the tract and the $y$-axis shows a negative logarithm of $p$values. The blue horizontal line in the plots represents the FDR-corrected threshold. Segments that pass the FDR-corrected threshold are considered significant. The second and fourth rows visualize $p$values mapped onto the 3D tracts. Dark orange colors imply lower $p$values and greater strength of association.

Significant effects were detected in the corticospinal tract left (FA), frontopontine tract left (FA), inferior longitudinal fasciculus right (MD), and middle longitudinal fasciculus right (AxD). MD, RD, and AD decrease. FA slightly increases. Fig. 6 highlights the significant tracts, with darker orange indicating areas of significant effects. The color gradient represents $p$values projected onto the 3D tracts, ranging from 1 to 0. Lighter colors indicate $p$values closer to 1 (no significant effects found), while darker colors indicate $p$values less than 0.05.

### 3.4. *APOE $\epsilon 3$ vs. APOE $\epsilon 4$*

We ran BUAN to assess the impact of $\epsilon 4$ on 38 major white matter tracts using 310 $\epsilon 3\epsilon 3$ (CN:191 MCI:85 Dementia:34) (140M, 170F) and 192 $\epsilon 3\epsilon 4/\epsilon 4\epsilon 4$ (CN:129, MCI:50, and Dementia:13) (88M, 104F) subjects from ADNI3 dataset.

Significant findings included frontopontine Tract left (FA), inferior Longitudinal Fasciculus right (AxD, MD), and Middle Longitudinal Fasciculus right (AxD), and spinothalamic tract left (MD), and right (AxD). MD decreases, AD changes vary along the length of the tract, with a slight increase in FA.

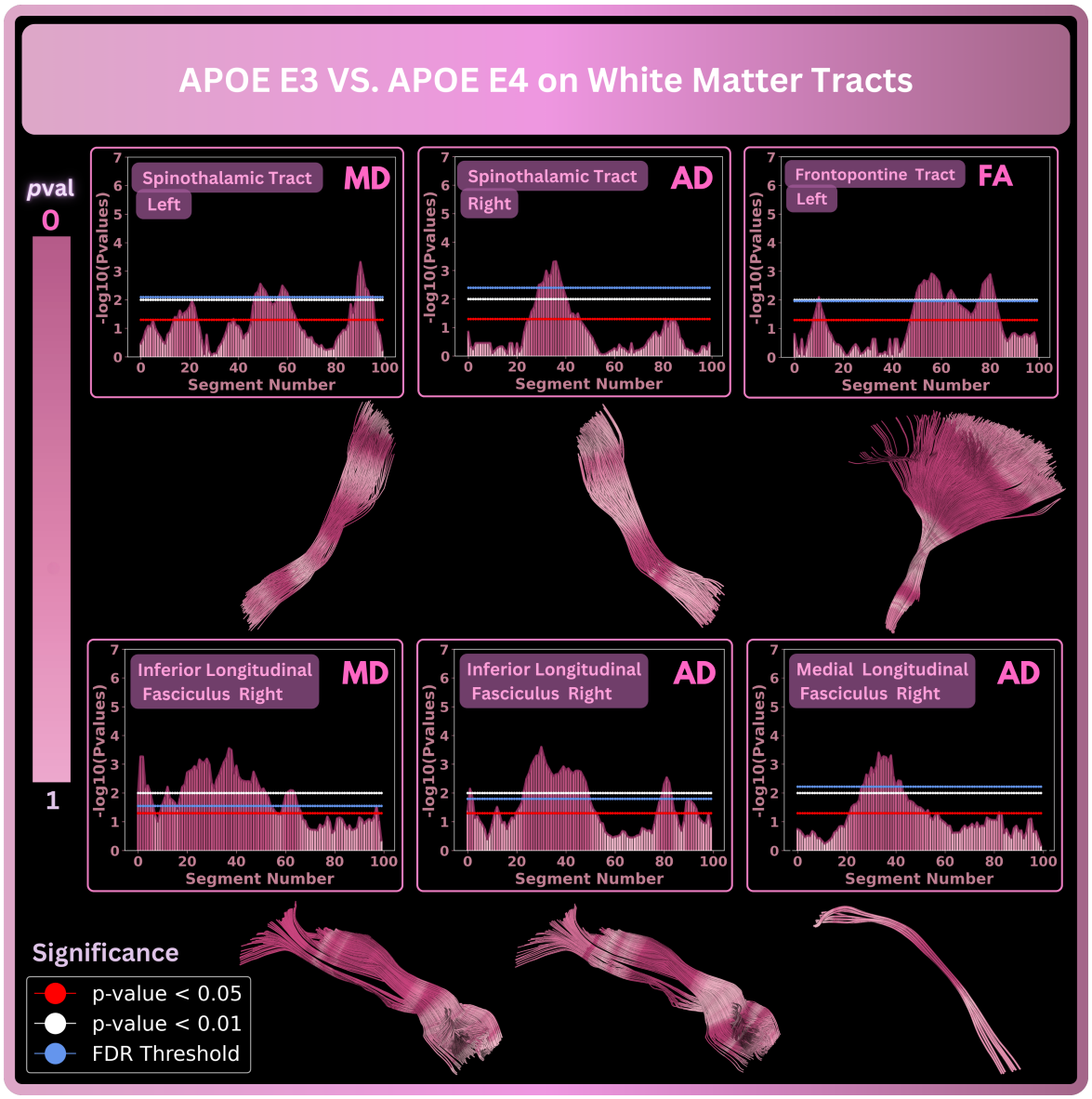


Fig. 7. BUAN results for group differences between $\epsilon 3\epsilon 3$ neutral gene and subjects with either $\epsilon 3\epsilon 4$ or $\epsilon 4\epsilon 4$ gene in white matter tracts . The first and third row shows $p$value plots for each tract, where the x-axis represents the segment number along the tract and the y-axis shows a negative logarithm of $p$values. The blue horizontal line in the plots represents the FDR corrected threshold. Segments that pass the FDR corrected threshold are considered significant. The second and fourth rows visualize $p$values mapped onto the 3D tracts. Where dark pink color implies lower $p$values and more significance.

Tract visualizations shown in Fig. 7 highlight the significant tracts, with darker pink indicating areas of significant effects. The color gradient represents $p$values projected onto the 3D tracts, ranging from 1 to 0. Lighter colors indicate $p$values closer to 1 (no significant effects detected), while darker colors indicate $p$values less than 0.05.

### 3.5. *APOE $\epsilon 3$ vs. APOE $\epsilon 2$*

We ran BUAN to assess the impact of the APOE $\epsilon 2$ genotype (which is protective against Alzheimer's disease) on 38 major white matter tracts using 310 $\epsilon 3\epsilon 3$ (CN: 191, MCI: 85, and Dementia: 34) (140M, 170F) and 48 $\epsilon 3\epsilon 2/\epsilon 2\epsilon 2$ 48, (CN: 33, MCI: 14, and Dementia: 1) (28M, 20F) participants in the ADNI3 dataset.

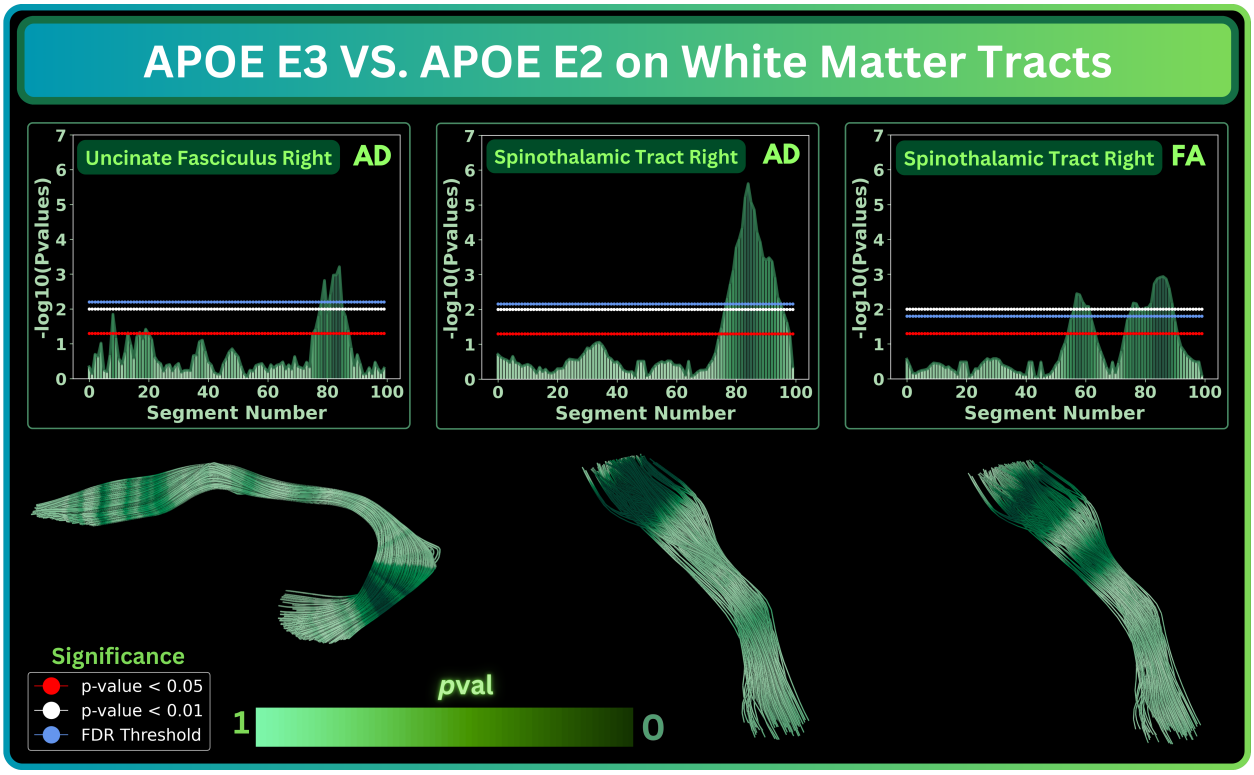


Fig. 8. BUAN results for group differences between the $\epsilon 3\epsilon 3$ (neutral) gene and participants with either $\epsilon 3\epsilon 2$ or $\epsilon 2\epsilon 2$ gene in white matter tracts. The first and third rows show $p$value plots for each tract, where the $x$-axis represents the segment number along the tract and the $y$-axis shows a negative logarithm of $p$values. The blue horizontal line in the plots represents the FDR-corrected threshold. Segments that pass the FDR-corrected threshold are considered significant. The second and fourth rows visualize $p$values mapped onto the 3D tracts. Where dark green color implies lower $p$values and greater significance.

We found the following tracts and measures to be significant: Middle Longitudinal fasciculus right (AxD), spinothalamic tract right (FA, AxD), and uncinate fasciculus right (AxD). FA increases, MD and RD decrease, and AxD changes vary along the length of the tracts. Tract visualizations shown in Fig. 8 highlight the significant tracts, with darker green indicating areas of significant effects. The color gradient represents $p$values projected onto the 3D tracts, ranging from 1 to 0. Lighter colors indicate $p$values closer to 1 (no significant effects found), while darker colors indicate $p$values less than 0.05.

## 4. Discussion

Our study employed the advanced tractometry method, BUAN (Bundle Analytics), to investigate the effects of amyloid, tau, APOE $\epsilon 4$, and APOE $\epsilon 2$ on the microstructure of white matter tracts in the brain. The results underscore the significant role of tau and amyloid as biomarkers for Alzheimer's disease (AD), revealing their profound impact on white matter integrity. Tau and amyloid deposition are associated with marked changes in MD, AD, and RD, with FA being the least sensitive metric. This highlights the critical nature of these biomarkers in the early detection and monitoring of AD progression.

Tau and amyloid significantly alter the microstructural properties of white matter tracts, which are essential for neural communication. APOE $\epsilon 4$ carriers showed microstructural changes consistent with poorer white matter integrity, compared to those with the $\epsilon 3/\epsilon 3$ genotype, in line with the heightened genetic risk for AD associated with APOE $\epsilon 4$. These alterations are likely due to the reduced efficiency of amyloid clearance and increased inflammation observed in $\epsilon 4$ carriers. Conversely, fewer white matter bundles were affected by APOE $\epsilon 2$, perhaps in line with its protective role against AD-related white matter degeneration.[?]

The findings also revealed that MD is the most affected metric, followed by AxD and RD, whereas FA is the least sensitive. This is consistent with prior literature studying the association of DTI metrics with dementia.[?,65] This differential sensitivity of diffusion metrics highlights the importance of selecting appropriate imaging markers for assessing white matter integrity in AD. MD, in particular, may serve as a more reliable indicator of microstructural damage in the context of AD pathology.

Our results underscore the significant role of the key Alzheimer's disease biomarkers in altering the microstructure of key neural pathways, with profound implications for understanding the progression and potential intervention points for AD. Some key tracts - the cingulum bundles and components of the corpus callosum - showed significant alterations in MD and RD in the presence of both amyloid and tau. The increased MD and RD indicate water molecules diffusing more freely in brain tissue - a sign of tissue degeneration and loss of cellular integrity typical in Alzheimer's disease. This diffusion behavior reflects the structural breakdown of neural pathways, which is critical in the progression of Alzheimer's disease.

Effects of amyloid and tau on crucial neural pathways, such as the cingulum and corpus callosum, may lead to impaired cognitive function and poorer interhemispheric communication. The cingulum bundle is critical for cognitive and emotional processing, and disruption of its microstructure can lead to impaired connectivity between the frontal lobe and other brain regions, contributing to the cognitive decline in AD patients.[66,67] The corpus callosum (CC), the largest white matter structure in the brain, facilitates inter-hemispheric communication. The impact on the corpus callosum (including forces major, forceps minor, and the middle sector of CC) is of great interest, as it plays a crucial role in coordinating cognitive and motor functions across the two brain hemispheres.[68] Additional tracts, such as the extreme capsule (EMC) and frontopontine tract (FPT), inferior longitudinal fasciculus (ILF), middle longitudinal fasciculus (ML), optic radiation (OR), and spinothalamic tract (STT), also exhibited significant changes in diffusivity metrics in relation to amyloid and tau. The EMC tract is located in the temporal lobe and is involved in auditory and language processing.[69] Damage

to this tract can affect communication and language abilities, common areas of decline in AD patients. The FPT connects the frontal cortex to the pons,[19] and its impairment can lead to issues with motor control and executive functions, which are often observed in AD. The ILF connects the temporal and occipital lobes, playing a role in visual processing and memory.[70] Disruptions in the ILF can contribute to visual memory deficits. The MLF is involved in language, semantic memory, and the integration of auditory and visual information.[71] Its impairment may contribute to semantic and memory deficits. OR carries visual information from the thalamus to the visual cortex, impairment in this tract can affect visual processing,[72] which is vital for spatial orientation and navigation. STT is critical for pain and temperature sensation.[73] While not typically associated with Alzheimer's core symptoms, its impairment could affect sensory processing. These findings suggest that the effects of AD are not confined to a single functional domain but instead disrupt multiple neural pathways, leading to the diverse clinical manifestations of the disease.

Moreover, this study highlights the limitations of earlier methods such as tract-based spatial statistics (TBSS),[29] which, despite identifying significant associations between amyloid positivity, clinical dementia severity, and specific brain regions[citations], suffers from limited resolution due to predefined atlas regions. The BUAN method overcomes these limitations by offering a finer-scale mapping of microstructural changes along the length of white matter tracts, providing a more detailed and accurate assessment of disease-related alterations. The pronounced effects detected in specific bundles reveal the vulnerability of these white matter fiber pathways to Alzheimer's disease pathology, highlighting their potential as biomarkers for early detection and monitoring of disease progression. Understanding how these tracts are compromised allows for more targeted research into therapeutic interventions to preserve or restore their integrity.

Future work will integrate microstructural measures derived from sophisticated modeling techniques, such as diffusion kurtosis imaging (DKI),[74] or neurite orientation dispersion and density imaging (NODDI)[75] into BUAN. Notably, NODDI shows superior ability in capturing the microstructural properties of brain tissue, outperforming traditional DTI metrics.[76]

## 5. Conclusion

In this study, we employ our advanced tractometry method, BUAN (Bundle Analytics), to evaluate the impact of amyloid, tau, APOE $\epsilon 4$, and APOE $\epsilon 2$ on the microstructural properties of white matter tracts in the brain. Among these factors, we find that microstructural alterations in white matter tracts are most significantly associated with tau and amyloid - the two prominent biomarkers of Alzheimer's disease. Fewer bundles are affected by APOE $\epsilon 2$, and comparing APOE $\epsilon 4$ with APOE $\epsilon 3/\epsilon 3$ reveals stronger microstructural alterations than comparing APOE $\epsilon 4$ with $\epsilon 2$ and $\epsilon 3$ variants combined.

## 6. Acknowledgement

This research was supported by the NIH (National Institutes of Health) under the AI4AD project grant U01 AG068057, grant numbers P41 EB015922, and RF1 AG057892. We would like to acknowledge the National Institute of Biomedical Imaging and Bioengineering under

award numbers R01 EB027585 and R01 EB017230.

## References


1. M. Goedert, M. Spillantini and R. Crowther, Tau proteins and neurofibrillary degeneration, *Brain pathology* **1**, 279 (1991).
2. J. Sepulcre, M. J. Grothe, F. d'Oleire Uquillas, L. Ortiz-Terán, I. Diez, H.-S. Yang, H. I. Jacobs, B. J. Hanseeuw, Q. Li, G. El-Fakhri *et al.*, Neurogenetic contributions to amyloid beta and tau spreading in the human cortex, *Nature medicine* **24**, 1910 (2018).
3. V. L. Villemagne, V. Doré, S. C. Burnham, C. L. Masters and C. C. Rowe, Imaging tau and amyloid-$\beta$ proteinopathies in alzheimer disease and other conditions, *Nature Reviews Neurology* **14**, 225 (2018).
4. C. R. Jack Jr, D. A. Bennett, K. Blennow, M. C. Carrillo, B. Dunn, S. B. Haeberlein, D. M. Holtzman, W. Jagust, F. Jessen, J. Karlawish *et al.*, Nia-aa research framework: toward a biological definition of alzheimer's disease, *Alzheimer's & dementia* **14**, 535 (2018).
5. C. Haass and D. J. Selkoe, Soluble protein oligomers in neurodegeneration: lessons from the alzheimer's amyloid $\beta$-peptide, *Nature reviews Molecular cell biology* **8**, 101 (2007).
6. J. Graff-Radford, E. M. Arenaza-Urquijo, D. S. Knopman, C. G. Schwarz, R. D. Brown Jr, A. A. Rabinstein, J. L. Gunter, M. L. Senjem, S. A. Przybelski, T. Lesnick *et al.*, White matter hyperintensities: relationship to amyloid and tau burden, *Brain* **142**, 2483 (2019).
7. T. Grimmer, M. Faust, F. Auer, P. Alexopoulos, H. Förstl, G. Henriksen, R. Perneczky, C. Sorg, B. H. Yousefi, A. Drzezga *et al.*, White matter hyperintensities predict amyloid increase in alzheimer's disease, *Neurobiology of aging* **33**, 2766 (2012).
8. C. Bancher, C. Brunner, H. Lassmann, H. Budka, K. Jellinger, G. Wiche, F. Seitelberger, I. Grundke-Iqbal, K. Iqbal and H. Wisniewski, Accumulation of abnormally phosphorylated $\tau$ precedes the formation of neurofibrillary tangles in alzheimer's disease, *Brain research* **477**, 90 (1989).
9. P. V. Arriagada, J. H. Growdon, E. T. Hedley-Whyte and B. T. Hyman, Neurofibrillary tangles but not senile plaques parallel duration and severity of alzheimer's disease, *Neurology* **42**, 631 (1992).
10. K. Kantarci, M. E. Murray, C. G. Schwarz, R. I. Reid, S. A. Przybelski, T. Lesnick, S. M. Zuk, M. R. Raman, M. L. Senjem, J. L. Gunter *et al.*, White-matter integrity on dti and the pathologic staging of alzheimer's disease, *Neurobiology of aging* **56**, 172 (2017).
11. Z. Li, F. Shue, N. Zhao, M. Shinohara and G. Bu, Apoe2: protective mechanism and therapeutic implications for alzheimer's disease, *Molecular neurodegeneration* **15**, p. 63 (2020).
12. M. J. Grothe, S. Villeneuve, M. Dyrba, D. Bartrés-Faz, M. Wirth, A. D. N. Initiative and A. D. N. Initiative, Multimodal characterization of older apoe2 carriers reveals selective reduction of amyloid load, *Neurology* **88**, 569 (2017).
13. E. H. Corder, A. M. Saunders, W. J. Strittmatter, D. E. Schmechel, P. C. Gaskell, G. Small, A. Roses, J. Haines and M. A. Pericak-Vance, Gene dose of apolipoprotein e type 4 allele and the risk of alzheimer's disease in late onset families, *Science* **261**, 921 (1993).
14. J. Van Bergen, X. Li, J. Hua, S. Schreiner, S. Steininger, F. Quevenco, M. Wyss, A. Gietl, V. Treyer, S. Leh *et al.*, Colocalization of cerebral iron with amyloid beta in mild cognitive impairment, *Scientific reports* **6**, p. 35514 (2016).
15. P. J. Basser, J. Mattiello and D. LeBihan, MR diffusion tensor spectroscopy and imaging, *Biophysical Journal* **66**, 259 (1994).
16. D. Le Bihan, J.-F. Mangin, C. Poupon, C. A. Clark, S. Pappata, N. Molko and H. Chabriat, Diffusion tensor imaging: concepts and applications, *Journal of Magnetic Resonance Imaging: An Official Journal of the International Society for Magnetic Resonance in Medicine* **13**, 534

(2001).
17. A. L. Alexander, J. E. Lee, M. Lazar and A. S. Field, Diffusion tensor imaging of the brain, *Neurotherapeutics* **4**, 316 (2007).
18. S. Farquharson, J.-D. Tournier, F. Calamante, G. Fabinyi, M. Schneider-Kolsky, G. D. Jackson and A. Connelly, White matter fiber tractography: why we need to move beyond dti, *Journal of neurosurgery* **118**, 1367 (2013).
19. M. Catani and M. T. De Schotten, A diffusion tensor imaging tractography atlas for virtual in vivo dissections, *cortex* **44**, 1105 (2008).
20. G. Gong, Y. He, L. Concha, C. Lebel, D. W. Gross, A. C. Evans and C. Beaulieu, Mapping anatomical connectivity patterns of human cerebral cortex using in vivo diffusion tensor imaging tractography, *Cerebral cortex* **19**, 524 (2008).
21. A. Yendiki, P. Panneck, P. Srinivasan, A. Stevens, L. Zöllei, J. Augustinack, R. Wang, D. Salat, S. Ehrlich, T. Behrens *et al.*, Automated probabilistic reconstruction of white-matter pathways in health and disease using an atlas of the underlying anatomy, *Frontiers in neuroinformatics* **5**, p. 23 (2011).
22. M. Cousineau, P.-M. Jodoin, E. Garyfallidis, M.-A. Côté, F. C. Morency, V. Rozanski, M. Grand'Maison, B. J. Bedell and M. Descoteaux, A test-retest study on parkinson's ppmi dataset yields statistically significant white matter fascicles, *NeuroImage: Clinical* **16**, 222 (2017).
23. B. Q. Chandio, S. L. Risacher, F. Pestilli, D. Bullock, F.-C. Yeh, S. Koudoro, A. Rokem, J. Harezlak and E. Garyfallidis, Bundle analytics, a computational framework for investigating the shapes and profiles of brain pathways across populations, *Scientific Reports* **10**, p. 17149 (2020).
24. B. Q. Chandio, T. Chattopadhyay, C. Owens-Walton, J. E. V. Reina, L. Nabulsi, S. I. Thomopoulos, E. Garyfallidis and P. M. Thompson, Fiberneat: Unsupervised white matter tract filtering, in *2022 44th Annual International Conference of the IEEE Engineering in Medicine & Biology Society (EMBC)*, 2022.
25. J. D. Yeatman, R. F. Dougherty, N. J. Myall, B. A. Wandell and H. M. Feldman, Tract profiles of white matter properties: automating fiber-tract quantification, *PloS one* **7**, p. e49790 (2012).
26. B. Q. Chandio, C. Owens-Walton, J. E. Villalon-Reina, L. Nabulsi, S. I. Thomopoulos, J. Guaje, E. Garyfallidis and P. M. Thompson, Microstructural changes in the white matter tracts of the brain due to mild cognitive impairment, *Alzheimer's & Dementia* **18**, p. e065339 (2022).
27. A. H. Zhu, T. M. Nir, S. Javid, J. E. Villalon-Reina, A. L. Rodrigue, L. T. Strike, G. I. de Zubicaray, K. L. McMahon, M. J. Wright, S. E. Medland *et al.*, Lifespan reference curves for harmonizing multi-site regional brain white matter metrics from diffusion mri, *bioRxiv* (2024).
28. J. E. Villalón-Reina, A. H. Zhu, T. M. Nir, S. I. Thomopoulos, E. Laltoo, L. Kushan, C. E. Bearden, N. Jahanshad and P. M. Thompson, Large-scale normative modeling of brain microstructure, in *2023 19th International Symposium on Medical Information Processing and Analysis (SIPAIM)*, 2023.
29. S. M. Smith, M. Jenkinson, H. Johansen-Berg, D. Rueckert, T. E. Nichols, C. E. Mackay, K. E. Watkins, O. Ciccarelli, M. Z. Cader, P. M. Matthews *et al.*, Tract-based spatial statistics: voxelwise analysis of multi-subject diffusion data, *Neuroimage* **31**, 1487 (2006).
30. S. I. Thomopoulos, T. M. Nir, J. E. Villalon-Reina, A. Zavaliangos-Petropulu, P. Maiti, H. Zheng, E. Nourollahimoghadam, N. Jahanshad and P. M. Thompson, Diffusion MRI metrics and their relation to dementia severity: effects of harmonization approaches, in *17th International Symposium on Medical Information Processing and Analysis*, (SPIE, Campinas, Brazil, December 2021).
31. A. Zavaliangos-Petropulu, T. M. Nir, S. I. Thomopoulos, R. I. Reid, M. A. Bernstein, B. Borowski, C. R. Jack Jr., M. W. Weiner, N. Jahanshad and P. M. Thompson, Diffusion MRI Indices and Their Relation to Cognitive Impairment in Brain Aging: The Updated Multiprotocol Approach in ADNI3, *Frontiers in Neuroinformatics* **13**, p. 2 (February 2019).

32. A. M. Racine, N. Adluru, A. L. Alexander, B. T. Christian, O. C. Okonkwo, J. Oh, C. A. Cleary, A. Birdsill, A. T. Hillmer, D. Murali *et al.*, Associations between white matter microstructure and amyloid burden in preclinical alzheimer's disease: a multimodal imaging investigation, *NeuroImage: Clinical* **4**, 604 (2014).
33. B. Q. Chandio, S. L. Risacher, F. Pestilli, D. Bullock, F.-C. Yeh, S. Koudoro, A. Rokem, J. Harezlak and E. Garyfallidis, Bundle analytics, a computational framework for investigating the shapes and profiles of brain pathways across populations, *Scientific Reports* **10**, p. 17149 (December 2020).
34. I. B. Gari, A. Ramesh, S. Javid, S. P. Gadewar, E. Nourollahimoghadam, S. I. Thomopoulos, P. M. Thompson, T. M. Nir, N. Jahanshad, A. D. N. Initiative *et al.*, Medial tractography analysis (meta) for white matter population analyses across datasets, in *2023 11th International IEEE/EMBS Conference on Neural Engineering (NER)*, 2023.
35. B. Q. Chandio, Advancing white matter tractometry of the brain using diffusion MRI and machine learning, PhD thesis, Indiana University2022.
36. J. W. Vogel, Y. Iturria-Medina, O. T. Strandberg, R. Smith, E. Levitis, A. C. Evans and O. Hansson, Spread of pathological tau proteins through communicating neurons in human alzheimer's disease, *Nature communications* **11**, p. 2612 (2020).
37. S. M. Landau, C. Breault, A. D. Joshi, M. Pontecorvo, C. A. Mathis, W. J. Jagust and M. A. Mintun, Amyloid-$\beta$ imaging with pittsburgh compound b and florbetapir: comparing radiotracers and quantification methods, *Journal of Nuclear Medicine* **54**, 70 (2013).
38. S. Landau, B. Thomas, L. Thurfjell, M. Schmidt, R. Margolin, M. Mintun, M. Pontecorvo, S. Baker, W. Jagust and A. D. N. Initiative, Amyloid pet imaging in alzheimer's disease: a comparison of three radiotracers, *European journal of nuclear medicine and molecular imaging* **41**, 1398 (2014).
39. S. M. Landau, M. A. Mintun, A. D. Joshi, R. A. Koeppe, R. C. Petersen, P. S. Aisen, M. W. Weiner, W. J. Jagust and A. D. N. Initiative, Amyloid deposition, hypometabolism, and longitudinal cognitive decline, *Annals of neurology* **72**, 578 (2012).
40. S. M. Landau, M. Lu, A. D. Joshi, M. Pontecorvo, M. A. Mintun, J. Q. Trojanowski, L. M. Shaw, W. J. Jagust and A. D. N. Initiative, Comparing positron emission tomography imaging and cerebrospinal fluid measurements of $\beta$-amyloid, *Annals of neurology* **74**, 826 (2013).
41. N. Jahanshad, P. V. Kochunov, E. Sprooten, R. C. Mandl, T. E. Nichols, L. Almasy, J. Blangero, R. M. Brouwer, J. E. Curran, G. I. de Zubicaray *et al.*, Multi-site genetic analysis of diffusion images and voxelwise heritability analysis: A pilot project of the ENIGMA–DTI working group, *Neuroimage* **81**, 455 (2013).
42. S. I. Thomopoulos, T. M. Nir, J. E. V. Reina, N. Jahanshad and P. M. Thompson, Diffusion MRI metrics of brain microstructure in alzheimer's disease: Boosting disease sensitivity with multi-shell imaging and advanced pre-processing: Neuroimaging/new imaging methods, *Alzheimer's & Dementia* **16**, p. e046654 (2020).
43. J. V. Manjón, P. Coupé, L. Concha, A. Buades, D. L. Collins and M. Robles, Diffusion weighted image denoising using overcomplete local PCA, *PLoS ONE* **8** (2013).
44. E. Garyfallidis, M. Brett, B. Amirbekian, A. Rokem, S. Van Der Walt, M. Descoteaux, I. Nimmo-Smith and D. Contributors, Dipy, a library for the analysis of diffusion MRI data, *Frontiers in Neuroinformatics* **8**, p. 8 (2014).
45. E. Kellner, B. Dhital, V. G. Kiselev and M. Reisert, Gibbs-ringing artifact removal based on local subvoxel-shifts, *Magnetic Resonance in Medicine* **76**, 1574 (2016).
46. J.-D. Tournier, R. Smith, D. Raffelt, R. Tabbara, T. Dhollander, M. Pietsch, D. Christiaens, B. Jeurissen, C.-H. Yeh and A. Connelly, MRtrix3: a fast, flexible and open software framework for medical image processing and visualisation, *Neuroimage* **202**, p. 116137 (2019).
47. S. M. Smith, Fast robust automated brain extraction, *Human Brain Mapping* **17**, 143 (2002).

48. M. Jenkinson, C. F. Beckmann, T. E. Behrens, M. W. Woolrich and S. M. Smith, FSL, *Neuroimage* **62**, 782 (2012).
49. J. L. Andersson and S. N. Sotiropoulos, An integrated approach to correction for off-resonance effects and subject movement in diffusion MR imaging, *Neuroimage* **125**, 1063 (2016).
50. N. J. Tustison, B. B. Avants, P. A. Cook, Y. Zheng, A. Egan, P. A. Yushkevich and J. C. Gee, N4itk: improved N3 bias correction, *IEEE transactions on medical imaging* **29**, 1310 (2010).
51. E. J. Canales-Rodríguez, A. Daducci, S. N. Sotiropoulos, E. Caruyer, S. Aja-Fernández, J. Radua, J. M. Yurramendi Mendizabal, Y. Iturria-Medina, L. Melie-García, Y. Alemán-Gómez *et al.*, Spherical deconvolution of multichannel diffusion MRI data with non-Gaussian noise models and spatial regularization, *PLoS ONE* **10**, p. e0138910 (2015).
52. G. Girard, K. Whittingstall, R. Deriche and M. Descoteaux, Towards quantitative connectivity analysis: reducing tractography biases, *Neuroimage* **98**, 266 (2014).
53. E. Garyfallidis, M.-A. Côté, F. Rheault, J. Sidhu, J. Hau, L. Petit, D. Fortin, S. Cunanne and M. Descoteaux, Recognition of white matter bundles using local and global streamline-based registration and clustering, *NeuroImage* **170**, 283 (April 2018).
54. F.-C. Yeh, S. Panesar, D. Fernandes, A. Meola, M. Yoshino, J. C. Fernandez-Miranda, J. M. Vettel and T. Verstynen, Population-averaged atlas of the macroscale human structural connectome and its network topology, *NeuroImage* **178**, 57 (September 2018).
55. B. Q. Chandio, E. Olivetti, D. Romero-Bascones, J. Harezlak and E. Garyfallidis, Bundlewarp, streamline-based nonlinear registration of white matter tracts, *bioRxiv* (2023).
56. E. Garyfallidis, M. Brett, M. M. Correia, G. B. Williams and I. Nimmo-Smith, Quickbundles, a method for tractography simplification, *Frontiers in Neuroscience* **6**, p. 175 (2012).
57. W. E. Johnson, C. Li and A. Rabinovic, Adjusting batch effects in microarray expression data using Empirical Bayes methods, *Biostatistics* **8**, 118 (2007).
58. J.-P. Fortin, N. Cullen, Y. I. Sheline, W. D. Taylor, I. Aselcioglu, P. A. Cook, P. Adams, C. Cooper, M. Fava, P. J. McGrath *et al.*, Harmonization of cortical thickness measurements across scanners and sites, *Neuroimage* **167**, 104 (2018).
59. B. Q. Chandio, J. E. Villalon-Reina, T. M. Nir, S. I. Thomopoulos, Y. Feng, S. Benavidez, N. Jahanshad, J. Harezlak, E. Garyfallidis and P. M. Thompson, Bundle analytics based data harmonization for multi-site diffusion mri tractometry, *bioRxiv* , 2024 (2024).
60. L. V. Hedges, A random effects model for effect sizes., *Psychological Bulletin* **93**, p. 388 (1983).
61. E. Garyfallidis, S. Koudoro, J. Guaje, M.-A. Côté, S. Biswas, D. Reagan, N. Anousheh, F. Silva, G. Fox and F. Contributors, Fury: advanced scientific visualization, *Journal of Open Source Software* **6**, p. 3384 (2021).
62. J. Neyman and E. S. Pearson, On the use and interpretation of certain test criteria for purposes of statistical inference part i, *Biometrika* **20**, 175 (1928).
63. O. J. Dunn, Multiple comparisons among means, *Journal of the American statistical association* **56**, 52 (1961).
64. Y. Benjamini and Y. Hochberg, Controlling the false discovery rate: a practical and powerful approach to multiple testing, *Journal of the Royal statistical society: series B (Methodological)* **57**, 289 (1995).
65. T. M. Nir, N. Jahanshad, J. E. Villalon-Reina, A. W. Toga, C. R. Jack, M. W. Weiner, P. M. Thompson, A. D. N. I. (ADNI *et al.*, Effectiveness of regional dti measures in distinguishing alzheimer's disease, mci, and normal aging, *NeuroImage: clinical* **3**, 180 (2013).
66. S. E. Rose, F. Chen, J. B. Chalk, F. O. Zelaya, W. E. Strugnell, M. Benson, J. Semple and D. M. Doddrell, Loss of connectivity in alzheimer's disease: an evaluation of white matter tract integrity with colour coded mr diffusion tensor imaging, *Journal of Neurology, Neurosurgery & Psychiatry* **69**, 528 (2000).
67. Y. Yang, K. Schilling, N. Shashikumar, V. Jasodanand, E. E. Moore, K. R. Pechman, M. Bilgel,

L. L. Beason-Held, Y. An, A. Shafer *et al.*, White matter microstructural metrics are sensitively associated with clinical staging in alzheimer's disease, *Alzheimer's & Dementia: Diagnosis, Assessment & Disease Monitoring* **15**, p. e12425 (2023).

68. S. E. Black, S. D. Moffat, C. Y. David, J. Parker, P. Stanchev and M. Bronskill, Callosal atrophy correlates with temporal lobe volume and mental status in alzheimer's disease, *Canadian Journal of Neurological Sciences* **27**, 204 (2000).
69. L. Concha, C. Beaulieu and D. W. Gross, Bilateral limbic diffusion abnormalities in unilateral temporal lobe epilepsy, *Annals of neurology* **57**, 188 (2005).
70. F. Agosta, R. G. Henry, R. Migliaccio, J. Neuhaus, B. L. Miller, N. F. Dronkers, S. M. Brambati, M. Filippi, J. M. Ogar, S. M. Wilson *et al.*, Language networks in semantic dementia, *Brain* **133**, 286 (2010).
71. N. Makris, D. N. Kennedy, S. McInerney, A. G. Sorensen, R. Wang, V. S. Caviness Jr and D. N. Pandya, Segmentation of subcomponents within the superior longitudinal fascicle in humans: a quantitative, in vivo, dt-mri study, *Cerebral cortex* **15**, 854 (2005).
72. H. Bridge, O. Thomas, S. Jbabdi and A. Cowey, Changes in connectivity after visual cortical brain damage underlie altered visual function, *Brain* **131**, 1433 (2008).
73. A. Craig, Pain mechanisms: labeled lines versus convergence in central processing, *Annual review of neuroscience* **26**, 1 (2003).
74. A. J. Steven, J. Zhuo and E. R. Melhem, Diffusion kurtosis imaging: an emerging technique for evaluating the microstructural environment of the brain, *American Journal of Roentgenology* **202**, W26 (2014).
75. H. Zhang, T. Schneider, C. A. Wheeler-Kingshott and D. C. Alexander, NODDI: practical in vivo neurite orientation dispersion and density imaging of the human brain, *Neuroimage* **61**, 1000 (2012).
76. T. M. Nir, J. E. Villalón-Reina, L. E. Salminen, E. Haddad, H. Zheng, S. I. Thomopoulos, C. R. Jack Jr, M. W. Weiner, P. M. Thompson, N. Jahanshad *et al.*, Cortical microstructural associations with csf amyloid and ptau, *Molecular Psychiatry* , 1 (2023).